We are IntechOpen,
the world's leading publisher of
Open Access books
Built by scientists, for scientists

6,900
Open access books available

186,000
International authors and editors

200M
Downloads

Our authors are among the

154
Countries delivered to

TOP 1%
most cited scientists

12.2%
Contributors from top 500 universities

CLARIVATE ANALYTICS
BOOK CITATION INDEX
INDEXED

WEB OF SCIENCE™

Selection of our books indexed in the Book Citation Index
in Web of Science™ Core Collection (BKCI)

Interested in publishing with us?
Contact book.department@intechopen.com

Numbers displayed above are based on latest data collected.
For more information visit www.intechopen.com

Experimental and Numerical Study of the Flow Dynamics in Treatment Approaches for Aortic Arch Aneurysms

Asaph Nardi, Barak Even-Chen and Idit Avrahami

Additional information is available at the end of the chapter
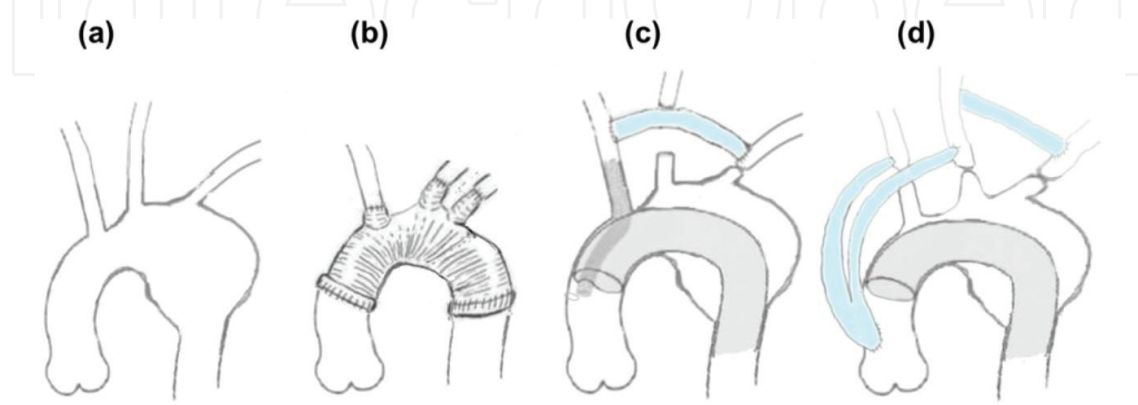
Abstract

Aortic arch aneurysm is a complex aortic pathology which affects one or more aortic arch vessels. In this chapter, we explore the hemodynamic behavior of the aortic arch in aneurysmatic and treated cases with three currently available treatment approaches: surgery graft, hybrid stent-graft and chimney stent-graft. The analysis included time-dependent experimental and numerical models of aneurysmatic arch and of the surgery, hybrid and chimney endovascular techniques. Dimensions of the models are based on typical anatomy, and boundary conditions are based on typical physiological flow. Flexible and transparent experimental models were used on a mock circulation in vitro experimental system to allow both visualization and time-dependent flow and pressure measurements. The simulations used computational fluid dynamics (CFD) methods to delineate the time-dependent flow dynamics in the four geometric models. Results of velocity vectors, flow patterns, pressure and wall shear stress distributions are presented. Both the numerical and experimental results agree on the poor hemodynamics of the aortic arch aneurysm and present the hemodynamic advantages of the surgery technique, implying the possible advantage of fenestrated stent-graft for the aortic arch. Out of the two minimally invasive procedures, the hybrid procedure clearly exhibits better hemodynamic performances. The chimney graft technique is based on off-the-shelf devices; thus, it is low in cost and requires less pre-operation preparations. However, it is associated with higher risks for complications, such as endoleaks and stroke. This chapter may give some insight into the hemodynamic characteristics of the different procedures.

Keywords: thoraces aortic aneurysm, endovascular repair, stent-graft, CFD, in vitro visualization

1. Introduction

Aortic arch aneurysm is a rare condition of aortic aneurysm with relatively high fatal risk for fast enlargement and rapture [1–3]. Aortic arch aneurysms or thoracoabdominal aneurysm (that involves large portions of the aorta) are considered complex aortic pathologies require coverage of one or more aortic arch vessels (as sketched, for example, in **Figure 1a**) and are usually repaired using total vessel replacement via open surgery (as sketched in **Figure 1b**).

Figure 1. Schematic illustrations of aortic arch with: (a) aneurysm; (b) surgery graft; (c) chimney SG and (d) hybrid graft.

The introduction of endovascular aneurysm repair (EVAR) offers an attractive minimally invasive alternative for diseases of the aortic aorta. This technology has advanced to treat more complicated cases of aneurysm thanks to advances in imaging and materials technology. The surgical procedure for aortic arch replacement is considered one of the most challenging cardiac surgeries, which often requires a combination of median sternotomy and lateral thoracotomy and usually requires aortic cross-clamping and hypothermic circulatory arrest. It is a highly complex operation which carries a substantial risk of morbidity and mortality [4, 5]. The EVAR alternative, on the other hand, is a procedure that requires only small incisions in the groin, local anesthesia and without interrupting blood flow. EVAR procedures are associated with a lower morbidity and mortality compared to open repair technique [6–8].

However, EVAR techniques face a major challenge in the repair of the aortic arch, which is to maintain blood flow to the side branches in the sealing zone of the graft [9]. Since this condition is relatively rare and complicated, no standard clinically approved device was introduced yet and most of the reported clinical solutions to overcome this challenge are patient specific in house combination that can fall into one of the two major approach classifications: (i) the graft procedures using fenestrations or chimney technique (e.g., chimney of innominate artery, as sketched in **Figure 1c**), or (ii) the total hybrid debranching procedures (**Figure 1d**) [10].

In the chimney graft technique [7, 11, 12], a covered stent is placed parallel to the main aortic stent-graft, similar to a chimney, providing the necessary blood perfusion to the vital upper branches. In order to distribute the blood flow among the other upper branches, bypasses are also required between the side branches. For example, a bypass between the innominate artery (IA) and the left subclavian artery (LSA) and between the LSA and the left common carotid

artery (LCCA), as shown in **Figure 1c**. The chimney graft technique allows the use of standard off-the-shelf covered stents for an emergency or immediate treatments of challenging aneurysms without sufficient neck, allowing an alternative to fenestrated stent-grafts in urgent cases [13].

In the hybrid total aortic arch debranching, a bifurcated Dacron graft is connected to the ascending aorta using a proximal end-to-side anastomosis [14–17]. The deployment of the endograft is done after bypassing the LSA as shown in **Figure 1d**.

Both approaches were proven to be technically feasible with high short-term technical success rate and relatively favorable rates of perioperative outcomes. Long-term outcomes remain undefined [12, 18–20]. The hybrid technique is considered to have better performance [21]; however, it uses custom-made devices associated with long manufacturing times and increased costs [22]. The chimney technique has the advantage of applying available off-the-shelf devices, being technically less complicated. However, in high-risk patients, it is associated with a relevant morbidity, mortality and reintervention rate. Therefore, it is often recommended only for patients not suitable for conventional aortic arch repair or emergency cases at present [23, 24].

In this study, we show the similarities between the numerical mesh and the visualization models, thus properly representing the case, while obtaining similar flow patterns and regimes.

2. Methods

2.1. Experimental models

Four silicone prototype models were procured by dipping, representing typical anatomical geometries of the four cases. A hybrid graft was manually fitted using Propoxy 20 as seen in **Figure 2a**, to modify the healthy case. **Figure 2b** displays the resulted hybrid model after being fitted with the hybrid graft and a placement of a bypass between the LCCA and LSA. Note the clipping of the LCCA and IA arteries at their connection point to the aortic arch according to surgery specs using silicone glue.
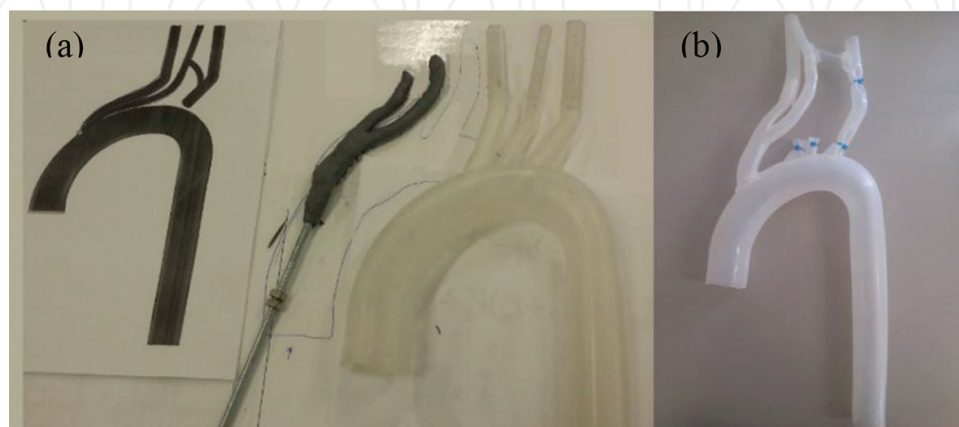
Figure 2. (a) Fitting the hybrid bypass mold to the real size model according to surgery specifications and (b) the resulted model.
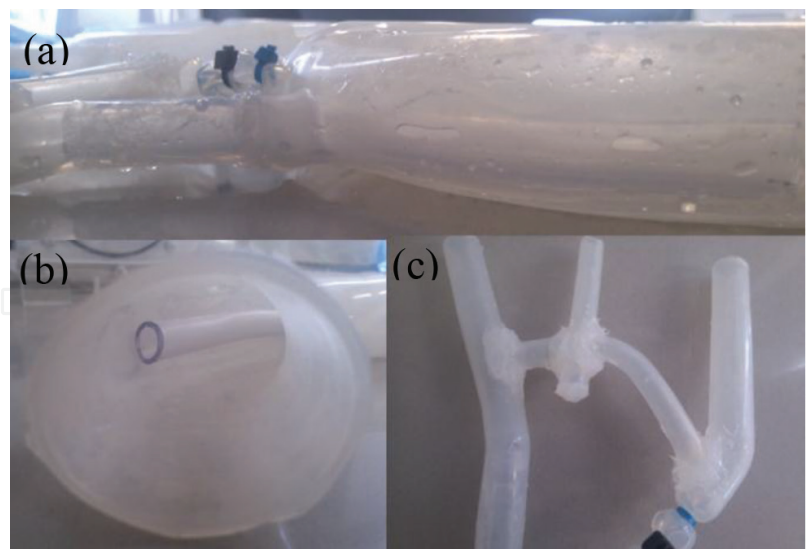
Figure 3. Remodeling the original model to match the chimney technique. Note the: (a) insertion of the stent graft into the Aortic arch and IA, (b) the permanent placement of the inner tube modeling the SG and (c) the connection of the LSA and LCCA arteries to the IA via a bypass.

Modifying a healthy case model to a chimney graft model was done, by inserting a 10-mm diameter tube—representing a stent-graft (SG) from the IA down to the aortic arch as seen in **Figure 3a**. In order to enable the insertion, the IA was cut and reconnected to the aortic arch. **Figure 3b** shows the permanent placement of the inner tube representing a SG. Note the bypass connection to the various arteries using an adhesive.

After gluing all of the models and bypasses, every model underwent a pressure test to insure no endoleaks. The hybrid model during visual sealing verification prior to a pressure test is seen in **Figure 4a** and during a pressure test in **Figure 4b**. Note the stream of water leaking from the bypasses connection to the LSA.

The four finalized models are seen in **Figure 5**.
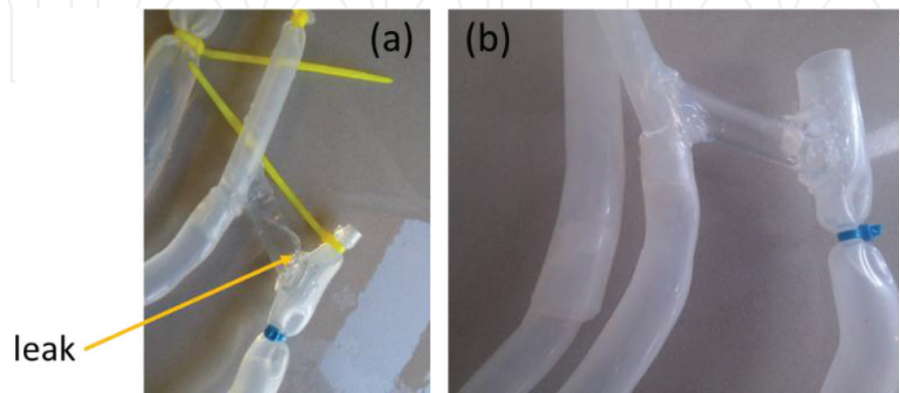
Figure 4. The hybrid model (a) during a pressure test. Note the leaking water stream at the bypasses connection point and (b) after fixing the leak.
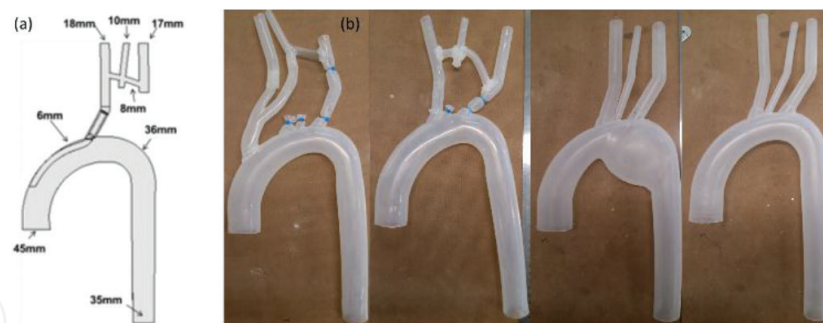
Figure 5. (a) Typical model dimensions and (b) the four silicone models.

2.2. Pulse duplicator flow loop and particle image set-up

An in vitro experimental set-up was utilized to create image aortic, graft and bypass flow. A pulse duplicator flow loop was constructed to generate pulsatile flow to mimic the physiological conditions of the arterial system using a positive displacement pump (enabler by hemo dynamics) as seen in **Figure 6a**. Each model was placed in turn into the system, where the aortic root was connected to a model of a three-leaflet aortic valve which was connected to a bubble trap and a pulse duplicator. A series of valves were placed at the IA, LSA, LCCA and descending aorta, respectively, to control pressure and flow rates as seen in **Figure 6b**. The mean inlet flow rate was set at 4 L/min at 60 beats per minute. Flow volume in the IA, LCCA and LSA was set to 0.4, 0.32 and 0.28 L/min, respectively, according to common physiological distribution rates. The IA, LCCA and LSA arteries were then reconnected to a reservoir.
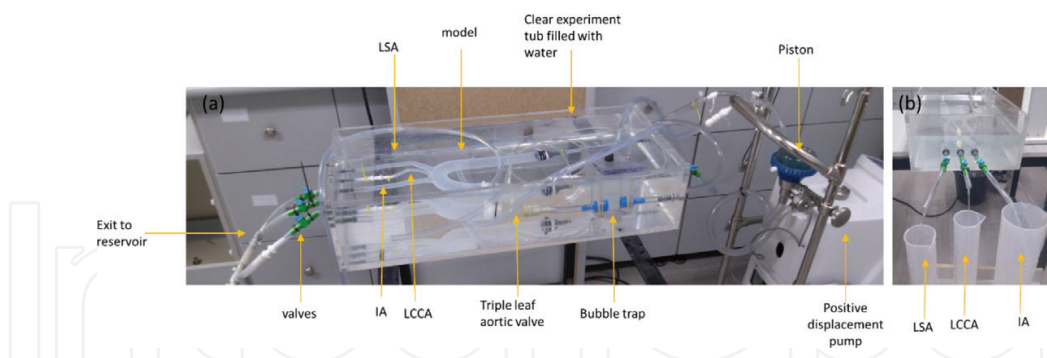

Figure 6. (a) The experimental system. The pulse duplicator is seen on the right and (b) measuring flow rates at the IA, LCCA and LSA.

Warm water (37°C) was utilized while letting the system work for several hours prior to the experiment in order to reduce the air solubility in the water.

A 532 nm laser with a diverging lens was placed at a distance to form a thin sheet of light. A high speed camera (Bonito, Allied vision technologies, Germany) was placed at a 90° angle beneath the model. Fluoresentric particles were then injected into the system, and videos and still shots were taken and analyzed.

2.3. Numerical analysis

The numerical model is fully described in previous publications [19] and is briefly described below. The numerical analysis included computational fluid dynamics (CFD) simulations of the time-dependent flow in models of the aneurysmatic arch and of the surgery, hybrid and chimney endovascular techniques (**Figure 7**), identical to the experimental models.
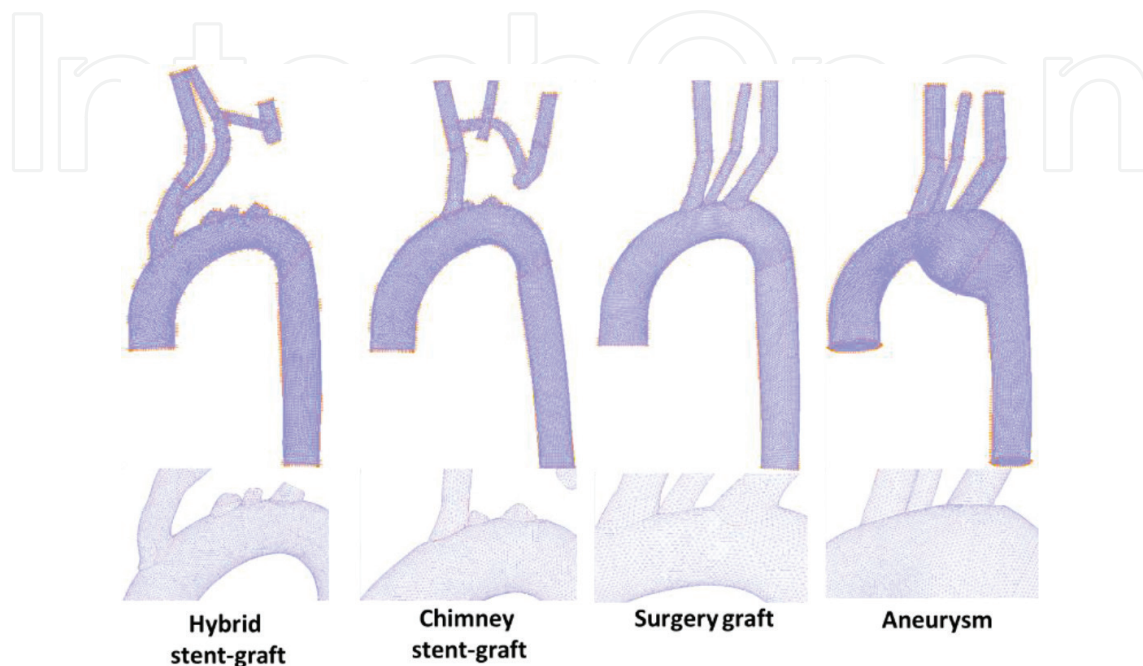
Figure 7. The four numerically meshed models (top—full models and bottom—magnified view).

The numerical model is fully detailed elsewhere [19] and will be presented here briefly. The model solves numerically the equations governing momentum and continuity in the fluid domain:

$$\nabla \cdot V = 0$$
$$\rho \frac{DV}{Dt} = -\nabla \, p + \mu \, \nabla^2 V + \rho \mathbf{g} \tag{1}$$

where p is static pressure, t is time, $\mathbf{V}$ is the velocity vector, ρ and μ are density and dynamic viscosity of the fluid, respectively, and $\mathbf{g}$ is the vector of gravity. The flow was assumed laminar and the fluid was assumed homogenous, incompressible (with density $\rho = 1$ g/mL) and Newtonian.

In order to compare the numerical models with the experiments, the simulations used water (with viscosity $\mu = 1$ cP). In addition, simulations with blood ($\mu = 3.5$ cP) were also performed.

The boundary conditions were similar to those specified for the experimental apparatus. The time-dependent inlet aortic flow and outlet pressure are shown in **Figure 8a**. Flow distribution between branches outlets was imposed as described in **Figure 8b**.

The commercial software ADINA (ADINA R&D Inc., MA) was used to solve the set of fluid equations using the finite-element scheme. The numerical meshes consisted of 0.5–1 M tetrahedral elements each. For each case, a single cardiac cycle was analyzed with 10 time steps per cycle. Mesh and time-step validation test were performed as detailed in previous reports [19].
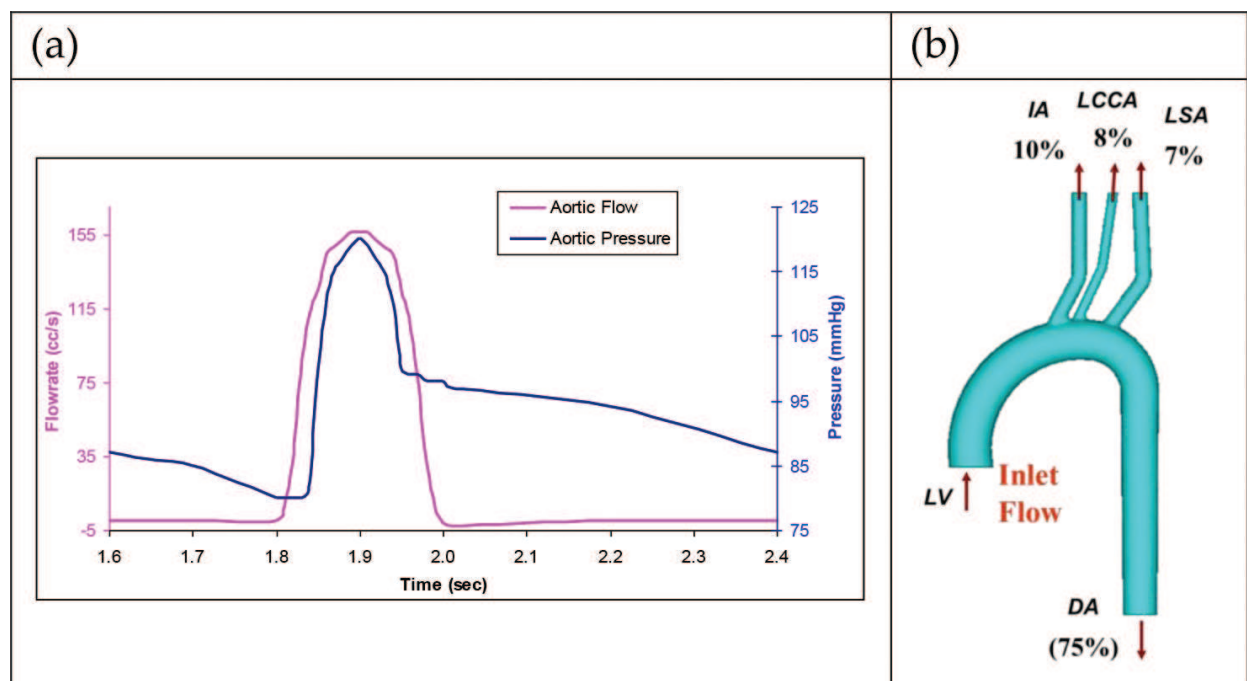
Figure 8. Boundary conditions of the numerical models: (a) inlet aortic flow and outlet pressure, as a function of time and (b) flow distribution between side branches (IA, innominate artery; LSA, left Subclavian artery; LCCA, left common carotid artery; DA, descending aorta).

3. Results

The resulted flow fields as calculated and visualized in the four cases are presented in **Figures 9–14**.

In the aneurysmatic case, three noticeable vortices are calculated (as seen in **Figure 9a**) and visualized (**Figure 9b**). In both methods, similar flow patterns dominant the flow field, including a
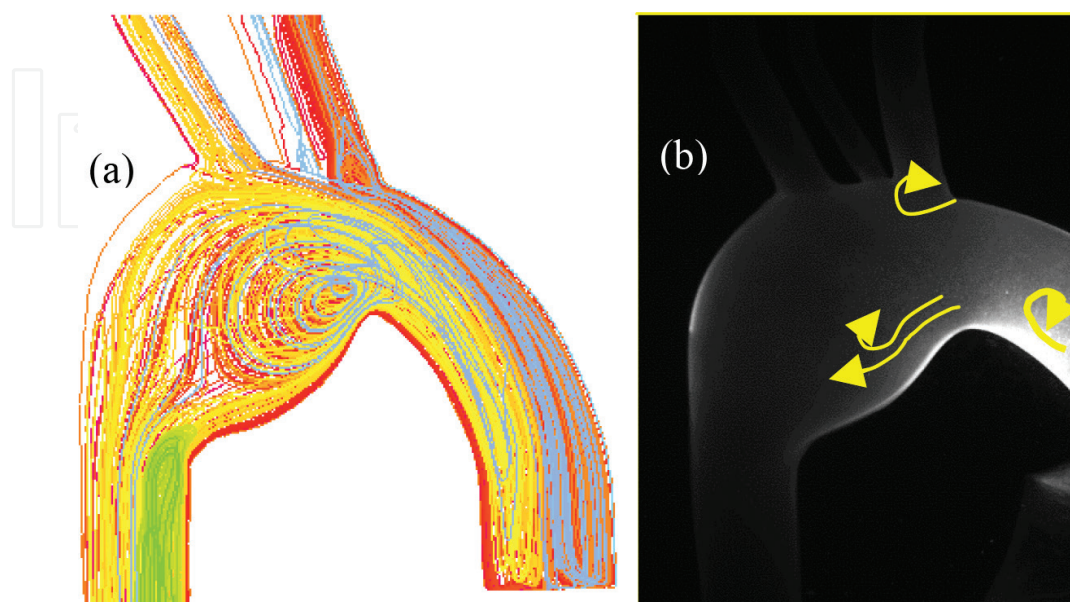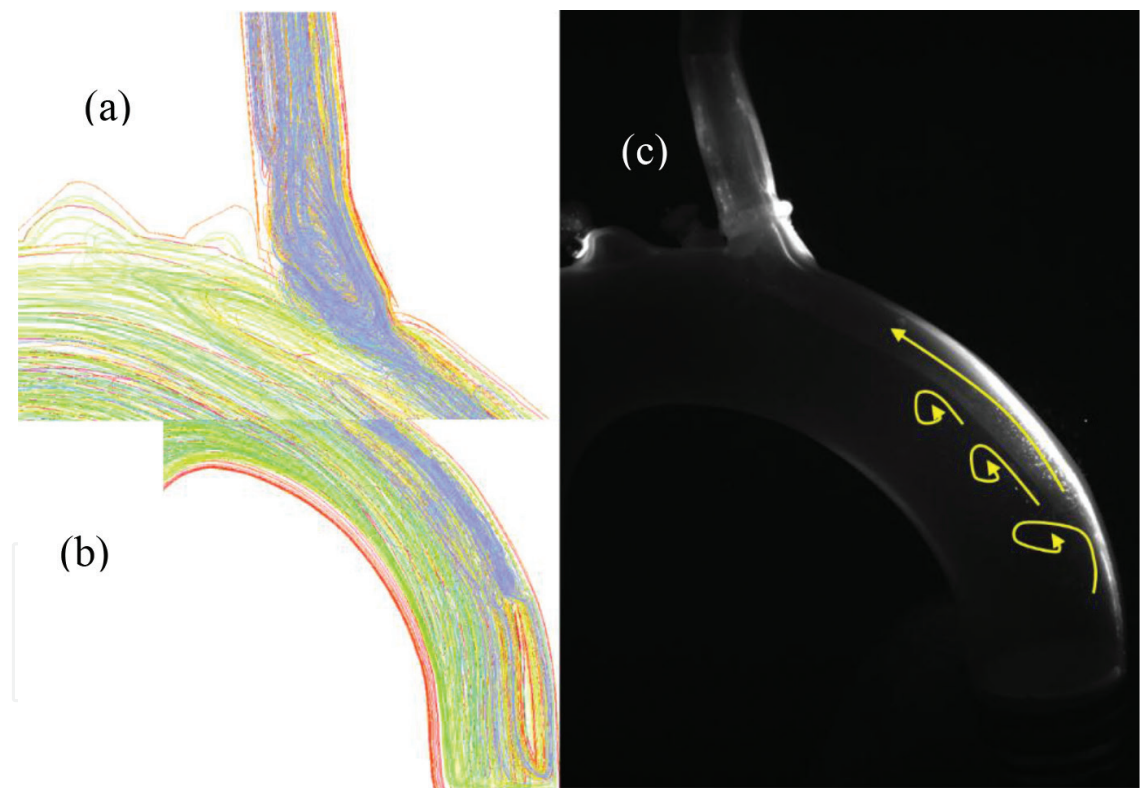

Figure 9. Flow patterns in the aneurysm case—(a) CFD particle trace and (b) visualization.
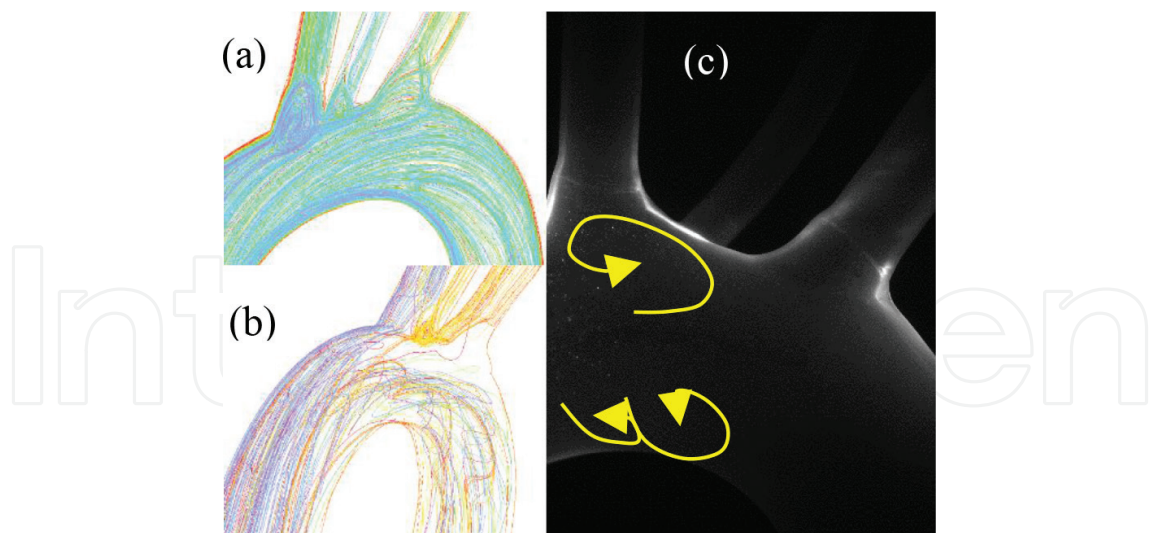
Figure 10. Flow patterns in the surgery graft. (a and b) CFD particle trace (c) visualization.

Figure 11. Flow patterns in the chimney graft (a) CFD particle trace at the IA branching (b) CFD particle trace in the aorta adjacent to the chimney graft (c) visualization.

single major vortex toward the center of the aneurysm accompanied by a shear layer between the vortex and the aneurysm wall. During diastole, a single vortex appears at the branching point of the IA with the aortic arch and a smaller vortex preceding the aneurysm.

Figure 10 shows flow patterns in the surgery graft case as calculated (a and b) and visualized (c). The branching arteries provoke vortices that form during the diastole. Helical flow starts near
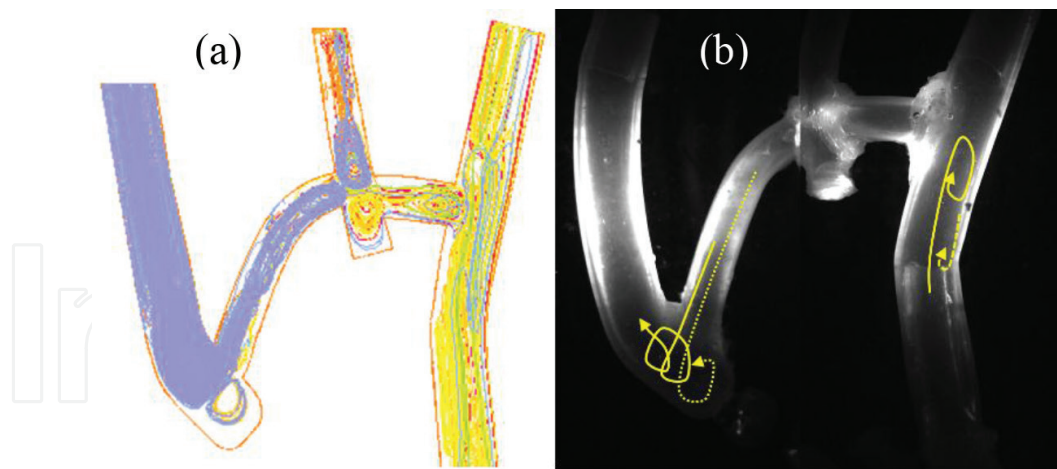
Figure 12. Flow patterns in the chimney bypass (a) CFD particle trace (b) visualization.
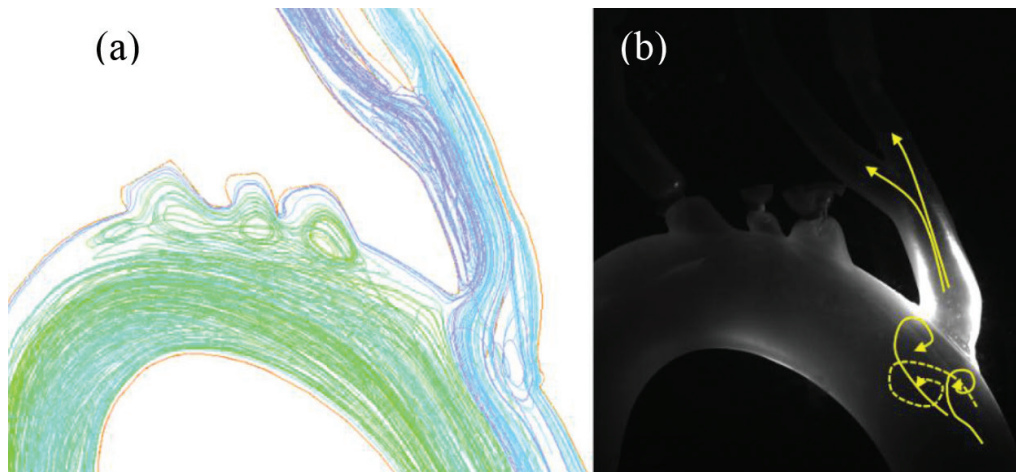
Figure 13. Hybrid graft (a) particle trace (b) visualization.

the branching arteries and down streams toward the descending aorta as seen in **Figure 10b**. A noticeable vortex appears at the branching point of the IA with the aorta. Two more vortices appear at the bottom section of the aortic arch where the helical flow is generated.

Figure 11 shows flow patterns in the chimney SG case as calculated (a and b) and visualized (c). Large vortices are found at the IA origin and at the SG's intake. Smaller vortices are formed adjacent to the SG.

The flow in the bypass connection with the IA, LCCA and LSA are shown in **Figure 12**. Vortices are found at the exit point from the SG to the IA, at the anastomosis to the LCCA and at the connection point of the bypass with the IA and LSA.

In the hybrid graft case (**Figure 13**), a vortex is seen at the branching point of the graft with the aorta. Smooth flow is seen in the graft and bifurcation. Vortices also appear at the stumps of the IA, LCCA and LSA. Vortices are also found at the bypass connection to the LCCA and LSA (**Figure 14**) and at the LSA stump.
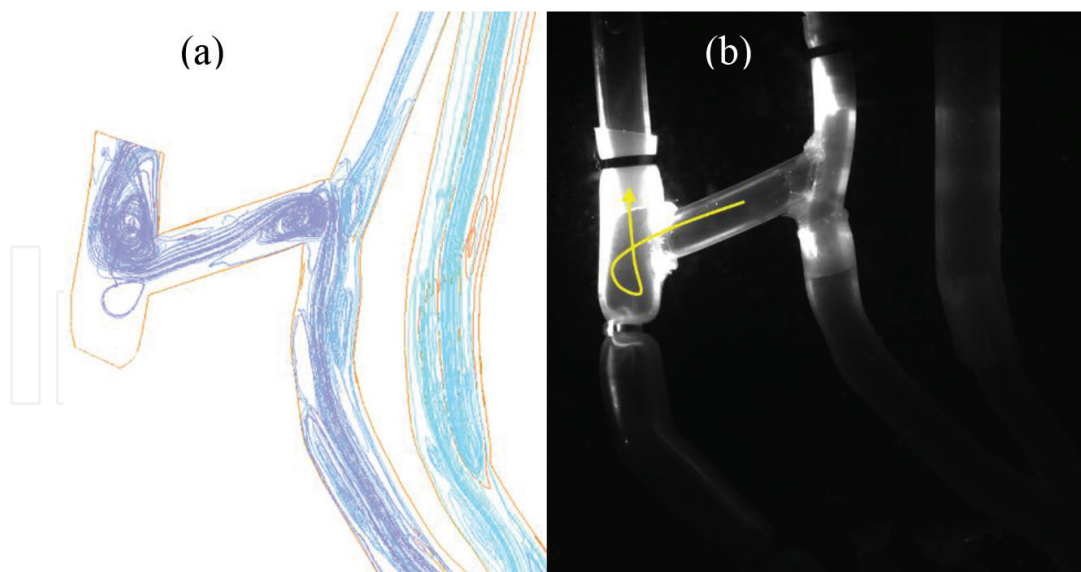
Figure 14. Hybrid bypass (a) CFD particle trace (b) visualization.

4. Discussion

In this study, four numerical models were built and verified using an in vitro experimental method. The models represent aortic arch aneurysm and three different treatment approaches. Comparison of flow patterns between the numerical and experimental results exhibits similar flow regimes in all four models, indicating the validity of the numerical model.

In the aneurysm case, poor hemodynamics is well demonstrated. A large vortex occupies the entire aneurysm sac, and in its center, a single significant stagnation point is observed, especially during diastole as seen in **Figure 9**. This induces poor particle washout and has a high risk of thrombus formation, as shown in previous studies as well [25, 26].

The surgery graft case demonstrated the best hemodynamics performance of all cases. The flow patterns deduced from the numerical analysis are clearly seen in the visualization (**Figures 9–14**). The helical flow that is generated at the aortic arch as seen in the numerical solution is noticed in vitro as well. This type of flow is consistent with findings from literature [27–29].

The chimney case (**Figures 11** and **12**) presented the most disturbed flow of all the three approaches. The large vortex at the insertion point of the stent-graft provokes a strong shear layer and vortical area downstream. A second large vortex at the bend toward the IA is well shown in the numerical model, but was not visually confirmed by the experiments due to local reflections and light scattering from the model. In addition, a series of vortices forming in the stubs of the arteries where they connect to the bypass are clearly seen numerically and experimentally (**Figure 12**).

In the hybrid graft case, a single vortex is noticed at the connection with the aortic arch (seen in **Figure 13**), followed by clean flow in the hybrid grafts branching point. Visualization confirms these findings. The bypass connection between the LSA and LCCA shows a vortex in the stub and is confirmed visually (**Figure 14**). Light did not reach the LCCA, and thus, visional confirmation was not possible.

This study is aimed at validating the numerical models using methods of visualization. The two methods were compared qualitatively by means of flow patterns analysis.

The resulted time-dependent flow presented similar flow regimes and vortex configurations.

The analysis did not take into consideration the motion of the aortic wall [30], and we did not use patient-specific geometries or boundary conditions. Nor turbulence or non-Newtonian effects were considered. Yet, we believe that our models represent the dominant factors influencing the hemodynamics in the different cases.

The reason for model simplifications is that patients' anatomy and physiology come in large variations, and whatever models used will lead to inaccuracy for the global analysis. Therefore, the models are based on representative prototype anatomical geometries, the boundary conditions are based on typical time functions from literature and the flow models were simplified. These assumptions might lead to some inaccuracies in the calculated values for specific patients, especially in WSS and pressure; however, it should not change the overall conclusions of the study.

In conclusion, this study was aimed at introducing a valid numerical model for the different cases. Future research will use more accurate experimental analysis and will examine flow parameters in the different numerical models, including specific regions (like gutter and stumps), wall shear stress, pressure drops and perfusion.

Author details

Asaph Nardi, Barak Even-Chen and Idit Avrahami*

*Address all correspondence to: iditav@ariel.ac.il

Ariel Biomechanics Center, Ariel University, Ariel, Israel

References

[1] Eric M. Isselbacher, *Thoracic and abdominal aortic aneurysms.* Circulation, 2005. 111(6): pp. 816–828.

[2] Eric M. Isselbacher, Epidemiology of thoracic aortic aneurysms, aortic dissection, intramural hematoma, and penetrating atherosclerotic ulcers, in *Aortic Dissection and Related Syndromes.* 2007, Springer US. pp. 3–15.

[3] Knowles, Andrew C., and John D. Kneeshaw. "Aortic dissection." Core Topics in *Cardiac Anesthesia*. 2nd ed. 2012: Cambridge University, UK. (2012): 223.

[4] Al Kindi, A.H., et al., *"Open" approach to aortic arch aneurysm repair.* Journal of the Saudi Heart Association, 2014. 26(3): pp. 152–161.

[5] Ziganshin, B.A. and J.A. Elefteriades, *Deep hypothermic circulatory arrest.* Annals of Cardiothoracic Surgery, 2013. 2(3): pp. 303–315.

[6]   Makaroun, M.S., et al., *Five-year results of endovascular treatment with the Gore TAG device compared with open repair of thoracic aortic aneurysms.* Journal of vascular surgery, 2008. 47(5): pp. 912–918.

[7]   Moulakakis, K.G., et al., *The chimney-graft technique for preserving supra-aortic branches: a review.* Annals of Cardiothoracic Surgery, 2013. 2(3): pp. 339–346.

[8]   Naughton, P.A., et al., *Emergent repair of acute thoracic aortic catastrophes: a comparative analysis.* Archives of Surgery, 2012. 147(3): pp. 243–249.

[9]   Avrahami, I., et al., *Hemodynamic and mechanical aspects of fenestrated endografts for treatment of Abdominal Aortic Aneurysm.* European Journal of Mechanics-B/Fluids, 2012. 35: pp. 85–91.

[10] Nardi, A., et al. Hemodynamical Aspects of Endovascular Repair for Aortic Arch Aneurisms. *ASME 2014 12th Biennial Conference on Engineering Systems Design and Analysis.* American Society of Mechanical Engineers, 2014.

[11] Ohrlander, T., et al., The chimney graft: a technique for preserving or rescuing aortic branch vessels in stent-graft sealing zones. *Journal of Endovascular Therapy* 15.4 (2008): 427–432.

[12] Cires, G., et al., *Endovascular debranching of the aortic arch during thoracic endograft repair.* Journal of Vascular Surgery, 2011. 53(6): pp. 1485–1491.

[13] Chuter, T.A.M., et al., *Modular branched stent graft for endovascular repair of aortic arch aneurysm and dissection.* Journal of Vascular Surgery, 2003. 38(4): pp. 859–863.

[14] Brinkman, W.T., W.Y. Szeto, and J.E. Bavaria, *Stent graft treatment for transverse arch and descending thoracic aorta aneurysms.* Current Opinion in Cardiology, 2007. 22(6): p. 510.

[15] Gottardi, R., et al., *An alternative approach in treating an aortic arch aneurysm with an anatomic variant by supraaortic reconstruction and stent-graft placement.* Journal of Vascular Surgery, 2005. 42(2): pp. 357–360.

[16] Ishimaru, S., *Endografting of the aortic arch.* Journal of Endovascular Therapy, 2004. 11(SupplementII): pp. 62–71.

[17] Saleh, H.M. and L. Inglese, *Combined surgical and endovascular treatment of aortic arch aneurysms.* Journal of Vascular Surgery, 2006. 44(3): pp. 460–466. e1.

[18] Yang, J., et al., *Endovascular chimney technique of aortic arch pathologies: a systematic review.* Annals of Vascular Surgery, 2012. 26(7): pp. 1014–1021.

[19] Nardi, A. and I. Avrahami, *Approaches for treatment of aortic arch aneurysm, A numerical study.* Journal of Biomechanics, 2016. BM-D-16-01127.

[20] Brand, M., et al., Clinical, Hemodynamical and Mechanical Aspects of Aortic Aneurisms and Endovascular Repair in Cardiology Research and Clinical Developments. 2013: Nova Publisher, NY.

[21] Buth, J., et al., Combined approach to stent-graft treatment of an aortic arch aneurysm. *Journal of Endovascular Therapy* 5.4 (1998): 329–332.

[22] Yoshida, R., et al., *Total endovascular debranching of the aortic arch.* European Journal of Vascular and Endovascular Surgery, 2011. 42(5): pp. 627–630.

[23] Geisbüsch, P., et al., *Complications after aortic arch hybrid repair.* Journal of Vascular Surgery, 2011. 53(4): pp. 935–941.

[24] Sugiura, K., et al., *The applicability of chimney grafts in the aortic arch.* Journal of Cardiovascular Surgery, 2009. 50(4): pp. 475–481.

[25] Gao, F., A. Qiao, and T. Matsuzawa "Numerical Simulation in Aortic Arch Aneurysm." *Reinhart Grundmann* 12 (2011): 207–222.

[26] Qiao, A., et al. Computational study of stented aortic arch aneurysms. 2005 *IEEE Engineering in Medicine and Biology 27th Annual Conference*. IEEE, 2006.

[27] Hugo, G.B. and H.B. Michael, *Blood flow measurements in the aorta and major arteries with MR velocity mapping.* Journal of Magnetic Resonance Imaging, 1994. 4(2): pp. 119–130.

[28] Morris, L., et al., *3-D numerical simulation of blood flow through models of the human aorta.* Journal of Biomechanical Engineering, 2005. 127: p. 767.

[29] Wen, C.Y., et al., *Investigation of pulsatile flowfield in healthy thoracic aorta models.* Annals of Biomedical Engineering, 2010. 38(2): pp. 391–402.

[30] van Prehn, J., et al., *Toward endografting of the ascending aorta: insight into dynamics using dynamic cine-CTA.* Journal of Endovascular Therapy, 2007. 14(4): pp. 551–560.